

Article

Non-Cooperative UAV Detection with Semi-Adaptive Sampling of Control Signal and SNR Estimation

Changce Wang ¹, Fangpei Zhang ², Wenjiang Ouyang ³, Xiaojun Jing ³ and Junsheng Mu ^{3,*}

¹ School of Automation and Electrical Engineering, University of Science and Technology, Beijing 100083, China; wangchant@sina.com

² Information Science Academy of China Electronics Technology Group Corporation, Beijing 100846, China; zhangfangpei@163.com

³ School of Information and Communication Engineering, Beijing University of Posts and Telecommunications, Beijing 100876, China; 691115650@bupt.edu.cn (W.O.); jxiaojun@bupt.edu.cn (X.J.)

* Correspondence: mujs@bupt.edu.cn

Abstract: This paper proposes a non-cooperative unmanned aerial vehicle (UAV) signal detection strategy based on a multichannel control signal with an energy detector (ED), wherein the sampling point of the control signal on each subchannel is adjusted with environmental signal-to-noise (SNR) in a semi-adaptive manner. In order to estimate the SNR in the environment, not only is a convolutional neural network (CNN) applied in the proposed signal detection strategy, but a long short-term memory network (LSTM) network is also included; in terms of features, it combines deep features and time-dimension features. The numbers of layers of the CNN and LSTM impact the performance of the algorithm. The decision on the presence or absence of a control signal is made at the fusion center (FC) based on the majority voting rule. This paper shows that the network with a two-layer CNN and a two-layer LSTM can achieve high estimation accuracy of environmental SNR. Simultaneously, the detection accuracy is improved by about 1 dB compared with the classical multichannel detection schemes.

Keywords: UAV detection; ED; majority voting; SNR estimation



Citation: Wang, C.; Zhang, F.; Ouyang, W.; Jing, X.; Mu, J. Non-Cooperative UAV Detection with Semi-Adaptive Sampling of Control Signal and SNR Estimation. *Electronics* **2022**, *11*, 1815. <https://doi.org/10.3390/electronics11121815>

Academic Editor: Carlos Tavares Calafate

Received: 11 May 2022

Accepted: 31 May 2022

Published: 8 June 2022

Publisher's Note: MDPI stays neutral with regard to jurisdictional claims in published maps and institutional affiliations.



Copyright: © 2022 by the authors. Licensee MDPI, Basel, Switzerland. This article is an open access article distributed under the terms and conditions of the Creative Commons Attribution (CC BY) license (<https://creativecommons.org/licenses/by/4.0/>).

1. Introduction

Over the past few years, unmanned aerial vehicles (UAVs) have been widely used in aerial photography, agriculture, plant protection, disaster relief, transportation, surveying and mapping, etc. [1–4]. The advanced technology behind 5G [5] further gives an impetus to the UAV industry. Cooperative UAVs bring great convenience to human life because they are under the surveillance of UAV management organization. Generally, UAVs can be categorized as cooperative UAVs and non-cooperative UAVs according to whether the surveillance platform has the flight trajectory information or communication link with the intruder. If there is no related information about a certain UAV, it is called a non-cooperative UAV. Although cooperative UAVs and most non-cooperative UAVs are under the power of their own controllers, collisions between non-cooperative UAVs and aircraft are increasing in frequency, which has caused great losses. Accordingly, it is a critical issue to detect surrounding UAVs in a non-cooperative manner, which has drawn increasing attention.

1.1. Related Work

Classical object detection methods include radar detection [6] and photoelectric detection [7], which face great challenges when applied to UAV detection. Specifically, the radar detection of UAV must deal with the low altitude, slow speed and small target problems, making it difficult for radars to capture UAVs. Similarly, when the distance between the UAV and photoelectric sensor is larger than 100 m, the UAV appears as several pixels in the final electro-optical image, especially in a hostile environment.

Usually, both the flight control system and the image transmission system of the UAV emit radio signals during the flight. Radio surveillance is used to detect and identify a UAV by monitoring its control signal and image transmission signal. Compared with radar detection and photoelectric detection, radio surveillance has four advantages. Firstly, it is not limited by UAV size, UAV material or occlusions. Secondly, there is no electromagnetic pollution in radio surveillance, and it can be used in long-term unattended UAV defense missions. Thirdly, the cost of radio surveillance is relatively low. Fourthly, it can be installed at a fixed point yet have a large range.

The surveillance scopes of photoelectric detection, radar detection and radio detection are illustrated as Figure 1. Photoelectric detection is appropriate for UAV detection with high accuracy, whereas its surveillance scope is the smallest. On the contrary, radio detection works as a rough scheme of UAV detection, and it only determines the presence or absence of a UAV. As a result, the surveillance scope of radio detection is the largest. When a UAV comes, radio detection firstly judges the presence or absence of UAV. If the UAV is detected, radars and photoelectric sensors start high-accuracy UAV detection. In this work, we focus on radio signal detection based on semi-adaptive sampling of the observed signal.

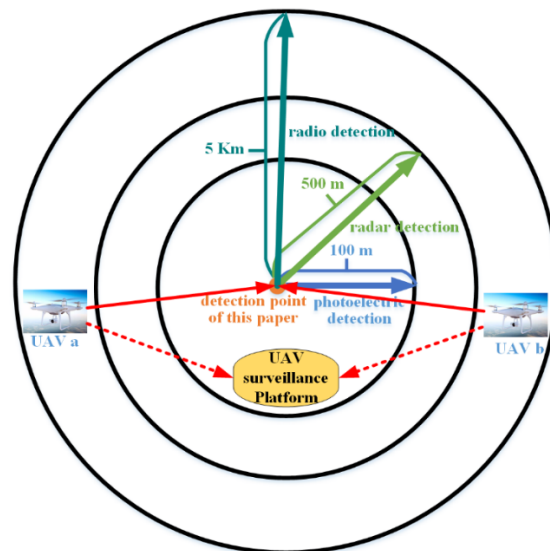


Figure 1. The surveillance scopes of multiple UAV detection schemes.

The surveillance radii of radio detection, radar detection and photoelectric detection are about 5 km, 500 m and 100 m, respectively. UAV a and UAV b denote the UAVs that have not been detected by the UAV surveillance platform, i.e., non-cooperative UAVs. The detection point of this paper in Figure 1 is trying to detect those non-cooperative UAVs with the proposed strategy.

To ensure the secrecy and avoid interference of communication, the control signal and image transmission signal of a UAV are frequency hopping (FH) signals with 2 MHz bandwidth. Special frequency bands are reserved for the transmission of control signals and image transmission signals, such as 840.5–845 MHz for uplink remote-control links; 1430–1444 MHz for downlink telemetry and information transmission links; and 2408–2440 MHz for the backup band in China. The central frequencies of the control and image transmission signals tend to be concentrated at 2.4 and 5.8 GHz in other countries. The key issue of radio-based UAV detection is how to detect a frequency hopping signal effectively. In the literature, FH signal detection schemes contain autocorrelation detection [8], power cancellation detection [9], adaptive multichannel detection [10], etc. Autocorrelation detection judges whether an FH signal exists based on a presupposed threshold from correlation analysis. However, the overdependence on the empirical threshold limits its application. Power cancellation detection works on the average power difference between

FH signal and interference. Its main defect is the high misjudgment probability when multiple FH signals coexist. Adaptive multichannel detection establishes a detection model for multiple sub-channels, and makes the final decision based on the fusion of local receivers. Nevertheless, its low detection performance limits its applications in practical systems, especially under strong noise conditions.

For a UAV signal detection scheme, environmental SNR estimation determines the sensing threshold and adaptive sampling points. The sensing threshold and adaptive sampling point determine the detection performance. Consequently, how to effectively estimate environmental SNR is the key factor for the proposed UAV detection scheme. In the literature, much work has been done on the issue of SNR estimation. A classical SNR estimation scheme contains maximum likelihood estimation (ML) [11], spectrum analysis estimation (SA) [12], etc. The main idea behind ML and SA is to evaluate the average power of the received signal or noise, respectively. An expectation-maximization (EM) approach was proposed in [13], where a good tradeoff is made between complexity and performance for medium-to-high SNRs. In [14], the data-aided (DA) SNR estimation was proposed for constant modulus modulations of time-variant flat Rayleigh fading channels, where the time-variant fading channel is modeled by considering the Jake model and the first order autoregressive (AR1) model.

With the great success of deep learning in natural image recognition, wireless signal processing technology based on deep learning has received more and more attention [15]. In [16], an SNR estimation scheme was proposed based on deep learning (DL), where a one-dimensional convolutional neural networks (CNN) is used for accurate SNR estimation. However, the correlation of time series signal has not been considered. To improve SNR estimation accuracy further, an SNR estimation scheme with CNN and long short-term memory (LSTM) network was proposed in [17], where the input data are one-dimensional and three-layer CNN and one-layer LSTM are utilized. Nevertheless, the influence from the layers of both CNN and LSTM are not considered.

To sum up, UAVs are low-altitude, slow and small targets. As a result, it is difficult for radars and photoelectric cameras to capture them far away. Radio detection can detect UAV object from far away, and ED is widely used in radio detection due to its low complexity. However, the detection performance declines rapidly when the environmental SNR is relatively low, especially below -5 dB, in ED-based detection schemes. Moreover, when the environmental SNR is relatively high, especially above 5 dB, the detection performance of ED-based schemes is high, always on the verge of 100%. In this case, the same sampling points as those of the low-SNR case are a waste of computing and storage resources, which also lowers the detection sensitivity for the UAV signal.

1.2. Motivation and Main Contribution

Motivated by the performance degradation at lower SNR and resource waste at higher SNR, this paper proposes an efficient, non-cooperative UAV signal detection scheme based on semi-adaptive sampling of the received signal. This is a classical multichannel signal detection issue [18]. For each subchannel, the environmental noise is assumed to be independent with mean zero and obey a Gaussian distribution hypothetically. In addition, the clean control signal on each subchannel is considered independent and to have a zero mean. As a result, the average energy of the received control signal can be modelled to follow the Gaussian distribution, and ED can be used to determine whether the control signal exists for each subchannel. Differently from the adaptive detection threshold scheme of ED, the sampling point of the received UAV signal on each subchannel adaptively varies with environmental SNR, if the variation of sampling point can make the detection performance high. Otherwise, the detection threshold adaptively varies with environmental SNR for the last sampling point. Furthermore, this paper proposes an SNR estimation network, where the features of the correlation between signal and noise are incorporated. In view of the tradeoff between estimation performance and estimation complexity, the proposed SNR estimation network contains a two-layer CNN and two layers of LSTM.

Finally, the fusion center provides the status of the control signal based on a certain fusion rule. The simulations indicate the proposed SNR estimation network outperforms the state-of-art, and the effectiveness of the proposed non-cooperative UAV detection scheme was validated.

2. System Model

In this section, we discuss the UAV signal detection system and formulate UAV signal detection as a multichannel signal detection problem. This paper considers the situation where a non-cooperative UAV is about to enter the observed area at a certain speed. The monitoring point of the non-cooperative UAV may be on the ground or on a UAV. Once the non-cooperative UAV enters the monitoring area, the radio detection equipment will start to scan and receive the control signal of the target UAV: each subchannel receives the control signal at the specific frequency and then determines whether it exists. The status of non-cooperative UAV is determined by the joint decisions of multiple subchannel detection.

The flow diagram of UAV signal detection is illustrated in Figure 2. Firstly, the observed signal of UAV is received by omnidirectional UWB antenna, and parallelly processed by multiple radio frequency (RF) chains. Then, an SNR estimation scheme based on a convolutional neural network (CNN) and a long short-term memory (LSTM) network is used for the ED-based decision of multiple local bands. Finally, local decision results are sent to the FC for the final decision based on fusion rules.

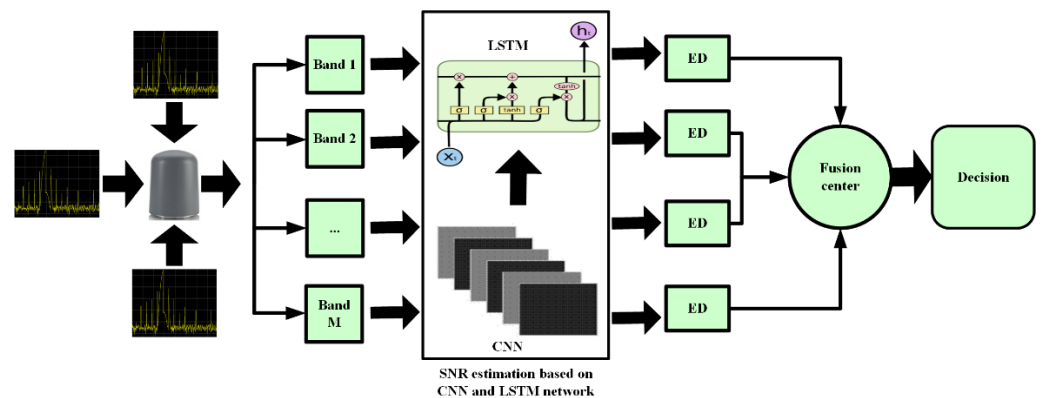


Figure 2. The flow diagrams of UAV signal detection based on adaptive sampling and the intelligent estimation of SNR.

Assume that observed signal $y_i(n)$ at the receiver of the i -th channel contains clean signal $s_i(n)$ and additive white Gaussian noise $x_i(n)$. Then,

$$y_i(n) = h_i(n)s_i(n) + x_i(n) \tag{1}$$

where $h_i(n)$ indicates the channel gain of the i -th channel and $|h_i(n)|$ follows a Nakagami distribution. $s_i(n)$ and $x_i(n)$ are independent and identically distributed random process with mean zero and variance σ_{s-i}^2 and σ_{x-i}^2 , respectively.

According to [19], the false alarm and detection probability of the i -th channel are given by

$$P_{f-i} = Q\left(\left(\frac{\epsilon_i}{\sigma_{x-i}^2} - 1\right)\sqrt{\tau_i f_{s-i}}\right), \tag{2}$$

$$P_{d-i} = Q\left(\left(\frac{\epsilon_i}{\sigma_{x-i}^2} - \gamma_i - 1\right)\sqrt{\frac{\tau_i f_{s-i}}{2\gamma_i + 1}}\right), \tag{3}$$

respectively, where τ_i is the sensing duration at a sensing event, f_{s-i} works as the sampling frequency, i is the detection threshold, $\gamma_i = \sigma_{s-i}^2 / \sigma_{x-i}^2$ represents received signal-to-noise

ratio (SNR) of the channel, $Q(x) = 1 - \Phi(x)$ denotes the complementary distribution function of a standard Gaussian $\Phi(x)$ and $Q(x) = \frac{1}{\sqrt{2\pi}} \int_x^{\infty} \exp(-\frac{t^2}{2}) dt$.

The observed FH signal $y(n)$ with all the channels can be formulated as

$$y(n) = \sum_{i=0}^{M-1} y_i(n) \quad (4)$$

where M denotes the number of hopping frequency number in a frequency hopping cycle and the duration of a cycle is generally short.

Compared with other kinds of FH signal, the main characteristics of a UAV signal [20] are summarized as follows.

- (1) The bandwidth of each hop keeps stable.
- (2) The residual time of each hop is the same.
- (3) The signal energy of each hop does not change during the residence time basically, and the signal energy of each hop is basically unchanged within the short sampling time.

As a result, the average energy of the received control signal at the i -th channel can be modelled to follow a Gaussian distribution, and ED can be used to determine whether the control signal exists.

3. Proposed Schemes

In this section, we present a UAV signal detection scheme based on multichannel signal detection and provide the false alarm probability and detection probability.

3.1. UAV Signal Detection with Semi-Adaptive Sampling

According to [18], the optimal sampling point is the function of the radio environment $(\gamma_i, \sigma_{x-i}^2)$ and sensing threshold (ϵ_i) . Reference [18] also indicates that, for the given i , the rise in sampling point can make up for the performance loss when the environmental SNR is small.

Meanwhile, assume signal variance σ_{s-i}^2 is constant and noise variance σ_{x-i}^2 is variable. When $\sigma_{u-i}^2 > \sigma_{x-i}^2$, $(P_{d-i})_{A-CFAR} > (P_{d-i})_{CFAR}$ under a certain fixed false alarm probability for the proposed strategy [18].

3.2. SNR Estimation Based on a CNN and an LSTM Network

One critical issue of UAV signal detection with adaptive sampling is the accurate and real-time estimation of environmental SNR. As a result, this subsection contributes to SNR estimation with deep learning. A neural network model is considered based on CNN and LSTM in this paper.

Note that classical SNR estimation schemes are inferior in accuracy and lower the detection performance of non-cooperative UAV in return. Although reference [16,17] have greatly improved the estimation accuracy based on a CNN module, the input data of [16,17] were one-dimensional, and the correlation between signal and noise was not considered. This paper proposes a two-dimensional CNN and LSTM network architecture based on [17] and considers the influences of the layers of CNN and LSTM on detection performance.

Figure 3 exhibits the network architecture of the proposed SNR estimation scheme. The received remote signal is framed and transformed into a two-dimensional signal by Topplitz transformation. Thereafter, CNN is considered to extract deep features, and LSTM is used for feature extraction in time sequences. Finally, the extracted features are combined with a fully connected layer and the estimated SNR is obtained.

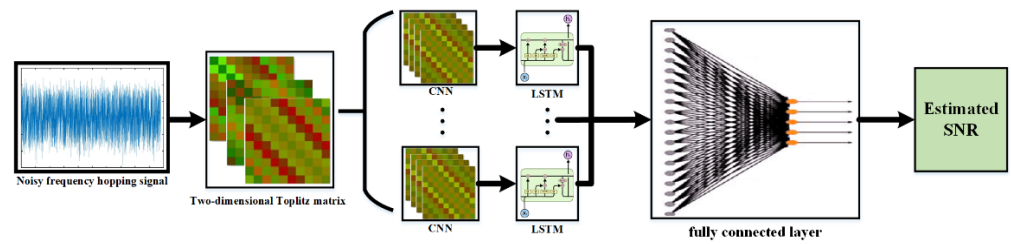


Figure 3. The overall network architecture of SNR estimation based on CNN and LSTM modules.

Assume that the length of the observed signal $y(n)$ at the receiver is L and the frame length is R . The two-dimension Toeplitz matrix can be denoted as

$$y(n) = \begin{pmatrix} y_{11}(n) & \cdots & y_{1R}(n) \\ \vdots & \ddots & \vdots \\ y_{R1}(n) & \cdots & y_{RR}(n) \end{pmatrix} \tag{5}$$

where $y_{1R}(n) = y_{R1}(n)$ denotes the correlation of the adjacent received signal.

Then, the CNN is applied to the two-dimensional Toeplitz matrix with convolution kernel size 3×3 and convolution stride 1. The main motivation of Toeplitz transform is to obtain the correlation of signal sequences so that more features can be incorporated into the network. Denote the shared weights of convolution kernel as $\omega(n)$. The output matrix after convolution operation can be written as

$$\bar{y}(n) = g(\omega(n)y(n) + b(n)), \tag{6}$$

where $g(\cdot)$ denotes the activation function of CNN, $\omega(n)$ represents the convolution kernel parameter and $b(n)$ signifies the bias. Note that the rectified linear unit (ReLU) is considered as the activation function in this paper due to its fast convergence and avoidable gradient explosion and gradient disappearance. In addition, the pooling layer is removed in this CNN network for possible feature loss.

LSTM is used in this paper to extract multidimensional features, including deep features of input signal sequences and the features of a time series signal, for higher SNR estimation accuracy. Let us define the current input, the last output of LSTM and the last unit state as \bar{y}_{t-1} , U_{t-1} and C_{t-1} . Additionally, the current output of LSTM and its corresponding unit state are denoted as U_t and C_t , respectively.

According to Figure 4, the LSTM module mainly contains three parts: the forget gate, input gate and output gate. The forget gate determines how much the unit state of the previous moment C_{t-1} is retained at the present moment C_t . Input gate determines how much the current input \bar{y}_t can be retained to the current unit state C_t , and the output gate determines how much the current unit state C_t can be outputted as the current output U_t .

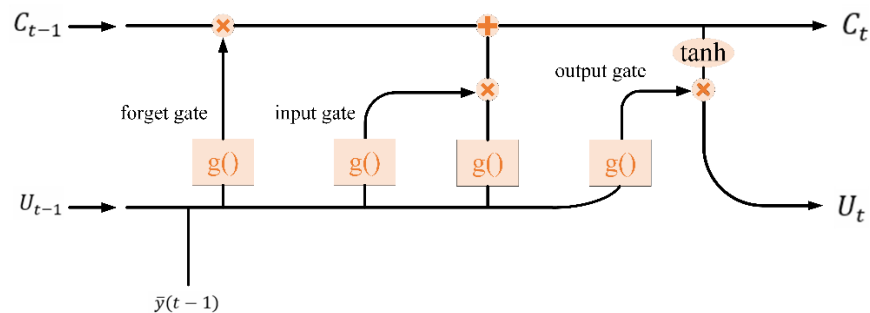


Figure 4. The architecture of an LSTM module (it contains a forget gate, input gate and output gate).

More specifically, the LSTM module mainly contains six procedures, as labeled in Figure 4.

- (1) The output of forget gate f_t can be described as

$$f_t = g(W_f \bar{y}_{t-1} + V_f U_{t-1} + b_f), \quad (7)$$

where W_f is the input weight of the forget gate, V_f is the weight of U_{t-1} and b_f denotes the corresponding bias.

- (2) The output of the input gate can be formulated as

$$i_t = g(W_i \bar{y}_{t-1} + V_i U_{t-1} + b_i), \quad (8)$$

where W_i is the input weight of the input gate, V_i is the weight of U_{t-1} and b_i denotes the corresponding bias.

- (3) The unit state of current input \bar{C}_t can be written as

$$\bar{C}_t = \tanh(W_c \bar{y}_{t-1} + V_c U_{t-1} + b_c), \quad (9)$$

$$\tanh(x) = \frac{\sinh(x)}{\cosh(x)} = \frac{e^x - e^{-x}}{e^x + e^{-x}}, \quad (10)$$

where W_c and V_c denote the corresponding weights, and b_c is the bias.

- (4) The unit state of current output C_t is defined as

$$C_t = f_t C_{t-1} + i_t g(\bar{C}_t). \quad (11)$$

- (5) The output of output gate o_t can be exhibited as

$$o_t = g(W_o \bar{y}_{t-1} + V_o U_{t-1} + b_o), \quad (12)$$

where W_o is the input weight of the input gate, V_o is the weight of U_{t-1} and b_o denotes the corresponding bias.

- (6) The output of current LSTM U_t can be denoted as

$$U_t = o_t \tanh(C_t). \quad (13)$$

3.3. UAV Signal Detection Based on Estimation SNR and Fusion Strategies

In this part, we discuss the training and testing of the proposed network in detail. To build the training set and test set, the required procedures were concluded as follows.

- (1) The remote signal sequence of UAV is generated under different SNRs (from -10 to 10 dB) based on MATLAB platform.
- (2) The remote signal sequence is divided into several short sequences with length 100.
- (3) The short sequence with length 100 is transformed into two-dimensional data by Toplitz transformation.
- (4) The obtained two-dimensional data are divided into two parts, training set and test training. The training set accounts for 70%, and the rest is the test set.

For the proposed SNR estimation network, the normalized mean square error (MSE) [21] works as the loss function, and it is defined as

$$\text{loss} = \frac{1}{K_0} \sum_{i=1}^{K_0} \frac{(snr_i - snr_i^{\text{predict}})^2}{(snr_i)^2}, k_0 \in [1, K_0], \quad (14)$$

where snr_i denotes the real SNR; snr_i^{predict} is the estimated SNR of the i -th channel; and K_0 means the number of the estimated SNR for the proposed network at a time and $K_0 = M$ in this paper.

The false alarm probability and detection probability are provided based on A-CFAR at the FC. Three fusion schemes are considered, namely, the AND rule, the OR rule and

the majority voting (MV) rule [19]. Assume the decision result of the i -th channel could be expressed as $D(i)$, where

$$D(i) = \begin{cases} 1 & \text{signal exists} \\ 0 & \text{signal is out} \end{cases} \quad (15)$$

Consequently, when the AND rule is used, the false alarm probability and detection probability could be described as

$$\begin{cases} (P_f)_{AND} = P(\sum_{i=1}^M D(i) = M|H_0) \\ (P_d)_{AND} = P(\sum_{i=1}^M D(i) = M|H_1) \end{cases}, \quad (16)$$

where M denotes the number of channels.

When the OR rule is considered, the false alarm probability and detection probability could be

$$\begin{cases} (P_f)_{OR} = P(\sum_{i=1}^M D(i) > 0|H_0) \\ (P_d)_{OR} = P(\sum_{i=1}^M D(i) > 0|H_1) \end{cases}, \quad (17)$$

When the MV rule is applied, the corresponding false alarm and detection probability could be respectively denoted as

$$\begin{cases} (P_f)_{MV} = \sum_{j=K}^M P(\sum_{i=1}^M D(i) > K|H_0) \\ (P_d)_{MV} = \sum_{j=K}^M P(\sum_{i=1}^M D(i) > K|H_1) \end{cases},$$

4. Simulation and Discussion

In this section, the simulations to validate the effectiveness of the proposed schemes are reported. Firstly, the accuracy of the proposed SNR estimation is exhibited. After that, the detection performance of the proposed method is shown and analyzed.

Note that the bit signal was randomly generated, and the corresponding baseband signal was obtained after the modulation of Minimum Frequency Shift Keying (MSK). Then the control signal of UAV was generated by MFSK modulation. The center frequency was 2.4 GHz and frequency-hopping bandwidth was set to 9.8 MHz with bit rate 50 kb/s. Additionally, the environmental SNR varied from -10 to 10 dB with step 1 dB. For each SNR, the obtained control signal was framed and transformed into a two-dimensional signal by Toeplitz transformation. Finally, the number of samples was 10,290, among which, 70% served as the training set and the rest were the test.

4.1. SNR Estimation Based on CNN and LSTM

To evaluate the SNR estimation precision, the absolute estimation error and relative estimation error were investigated. Assume the estimated SNR and real SNR are denoted as $SNR_{estimated}$ and SNR_{real} , respectively.

Figure 5 exhibits the relative error of SNR estimation for a fixed number of LSTM layers in the situation, while CNN layers vary from 2 to 4. $aCNN + bLSTM$ denotes a a -layer CNN network and b -layer LSTM network, where a and b are positive integers greater than 1.

The average relative error of SNR estimation is shown in Figure 5 with different numbers of CNN layers. Similarly to the above analysis, the relative error of SNR estimation with a four-layer CNN was even higher than that with a two-layer CNN. In view of computation complexity, a two-layer CNN is the optimal choice for SNR estimation in the proposed network architecture.

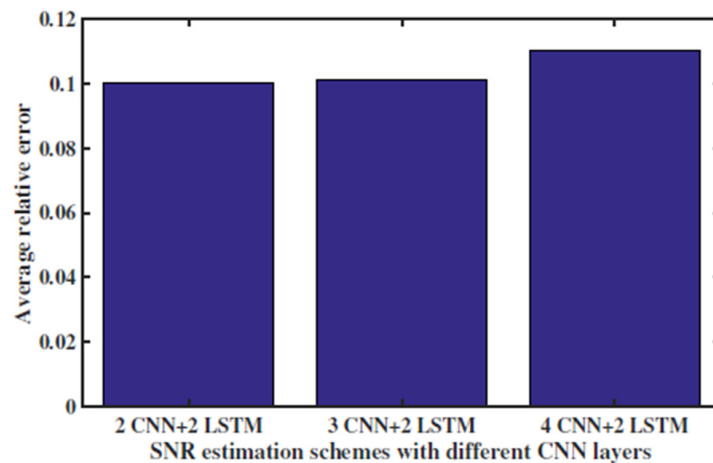


Figure 5. The average relative error of SNR estimation with different CNN layers (SNR varies from -10 to 10 dB).

Figure 6 exhibits the average relative error of SNR estimation with different numbers of LSTM layers and a fixed number of CNN in our architecture. According to Figure 6, the SNR estimation schemes based on deep learning are obviously superior to the classical schemes (SA and ML). This result indicates that deep learning-based methods can obtain higher quality features than classical ones and achieve higher evaluation accuracy of environmental SNR in return. On the other hand, as the number of LSTM layers increases, the relative error decreases at first and then keeps stable when the number of LSTM layers is equal or greater than two. This indicates that a two-layer LSTM is a superb choice for SNR estimation with two CNN layers.

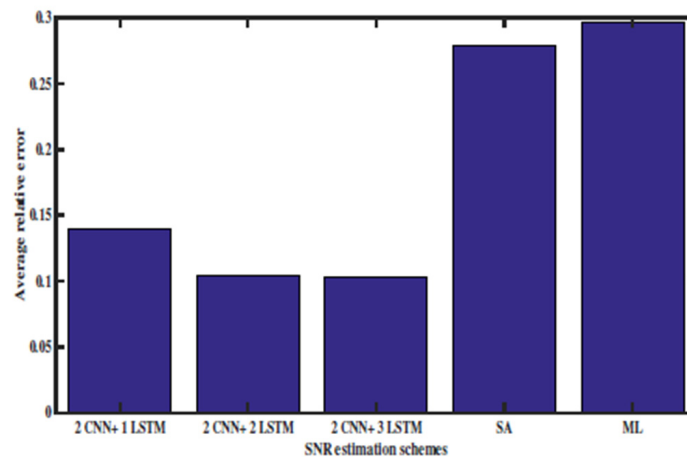


Figure 6. The average relative error of SNR estimation with different numbers of LSTM layers (SNR varies from -10 to 10 dB).

Figure 7 exhibits the absolute error of SNR estimation under the same conditions as Figure 6. Simultaneously, Figure 8 gives the corresponding average absolute error of SNR estimation. Figures 7 and 8 manifest the superiority of the proposed SNR estimation again, especially when two-layer LSTM and two-layer CNN are considered.

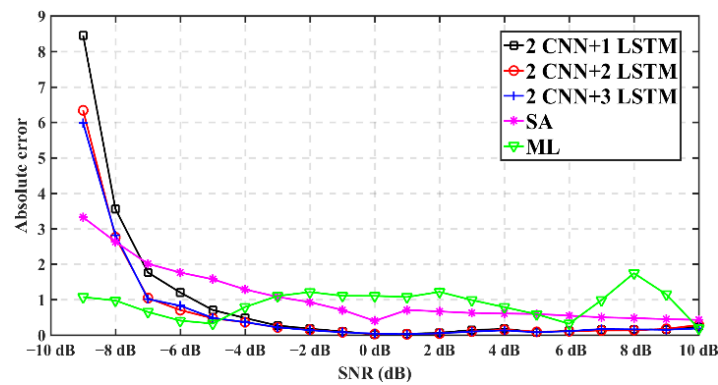


Figure 7. The absolute error of SNR estimation with different numbers of LSTM layers (SNR varies from -10 to 10 dB).

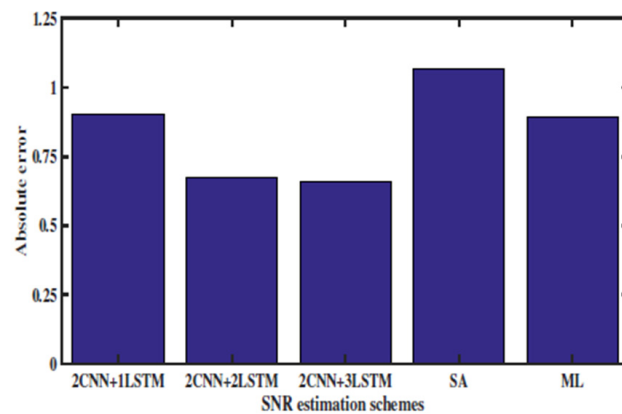


Figure 8. The average absolute error of SNR estimation with different numbers of LSTM layers (SNR varies from -10 to 10 dB).

In Figure 9, the absolute error comparisons between the proposed SNR estimation and the scheme in [17] are shown. In Figure 10, the absolute error of the proposed scheme is lower than that of the scheme in [17] when the environmental SNR is higher than -8 dB. This indicates that the SNR estimation accuracy of the proposed scheme is higher than that of the scheme in [17] in most cases.

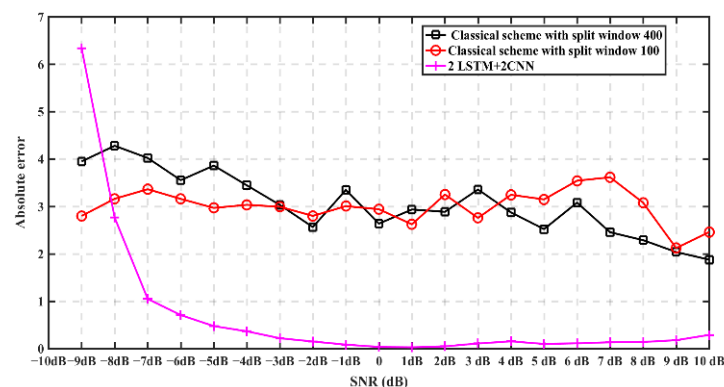


Figure 9. The absolute error comparisons of SNR estimation between the proposed scheme and classical scheme.

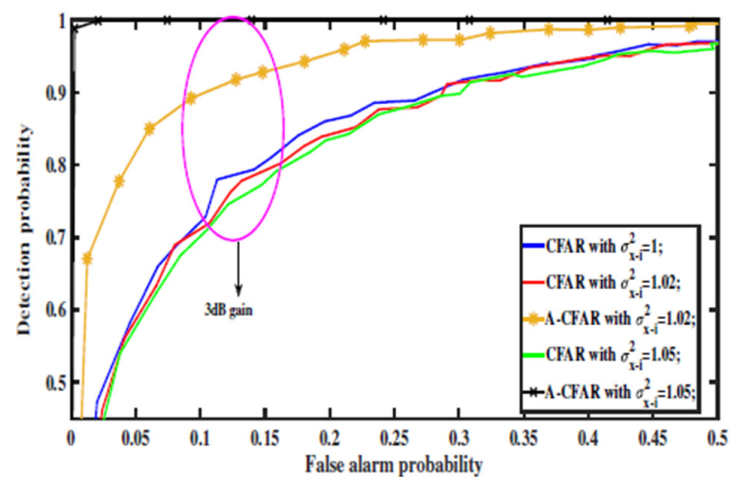


Figure 10. Performance comparison of CFAR and A-CFAR under various conditions.

To sum up, the SNR estimation architecture with a two-layer CNN and two-layer LSTM can effectively extract significant features of the observed signal frames and the correlated features in the time dimension, which leads to higher precision of SNR estimation for the observed remote signal. The accurate evaluation of environmental SNR contributes to adaptive sampling of remote signals and improves the detection performance of non-cooperative UAVs as a consequence.

4.2. SNR Estimation Based on CNN and LSTM

In this subsection, simulations are reported that examined the performance of the proposed scheme. The modulated signal of Minimum Shift Keying (MSK) [22,23] was chosen as the test signal on the i -th subchannel with center frequency $f_c = 2.44 \times 10^9$ Hz and sampling frequency $f_s = 6.0 \times 10^9$ Hz. The frequency of test signal varied from $f_c = 2.38 \times 10^9$ Hz to $f_c = 2.5 \times 10^9$ Hz, and bandwidth was $f_c = 2.0 \times 10^6$ Hz. A Rayleigh channel is considered with a Doppler shift of 250 in the simulations.

In the simulation, the modulated signal based on MSK was generated, and then Rayleigh fading and white Gaussian noise were added into the MSK signal. After the sampling and energy normalization of the noise-only case and the signal-plus-noise case, the detection and false alarm probability were obtained by the corresponding energy comparisons with the presupposed threshold. The simulation considered the scenario where a remote-control unit controls one non-cooperative UAV with a remote signal, and the presence or absence of non-cooperative is determined by the detection of the remote signal.

Figure 10 makes performance comparisons of CFAR and ACFAR on the i -th subchannel when σ_{x-i}^2 was 1 (SNR = -10 dB), 1.02 and 1.05, for fixed σ_{s-i}^2 . In Figure 10, the detection probability of A-CFAR is greater than that of CFAR for a given false alarm probability when $\sigma_{x-i}^2 = 1.02$ and $\sigma_{x-i}^2 = 1.05$.

In the Figures 11 and 12, the AND rule, OR rule and MV rule are considered to determine the presence or absence of remote signal at the FC while σ_{x-i}^2 is 1 (SNR = -10 dB), 1.02 or 1.05, for fixed σ_{s-i}^2 . From Figures 11 and 12, two conclusions are drawn. Firstly, the detection performance was greatly improved by the proposed A-CFAR compared to the classical CFAR. Secondly, the performance of A-CFAR with the MV rule was higher than with the AND rule or OR rule. As a result, the detection of the non-cooperative UAV was greatly improved with the proposed MV rule-based A-CFAR.

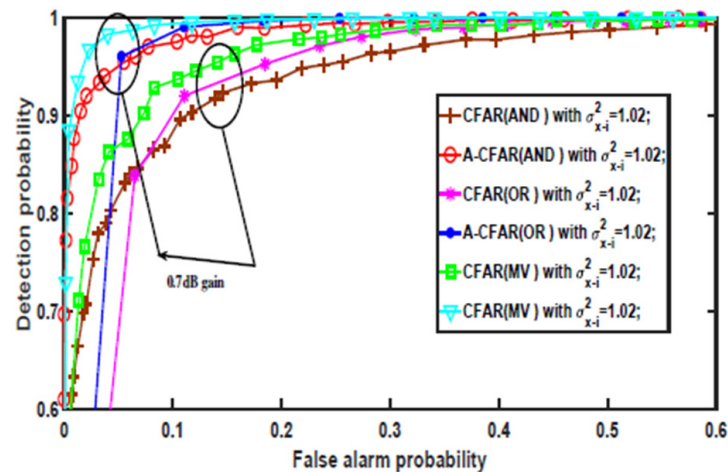


Figure 11. Decision results with various fusion rules ($\sigma_{x-i}^2 = 1.02$, $M = 3$).

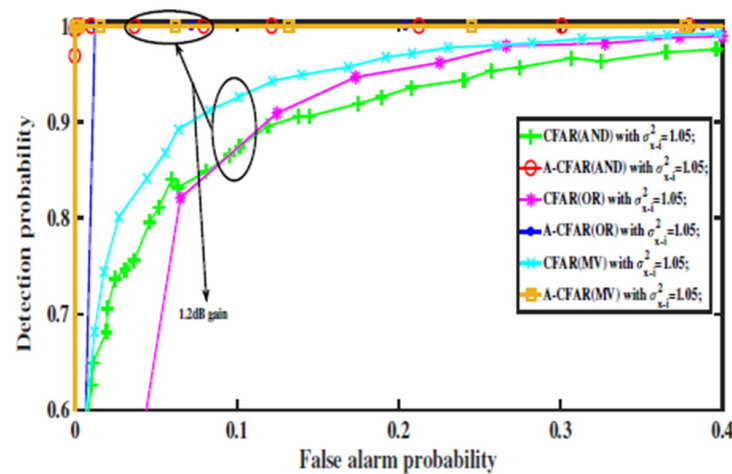


Figure 12. Decision results with various fusion rules ($\sigma_{x-i}^2 = 1.05$, $M = 3$).

Note that the remote-control distance of a non-cooperative UAV varies from 1 to 10 km according to UAV type [24]. As a result, the proposed detection scheme for a remote signal is effective within the distance scope mentioned above in theory.

5. Conclusions

In this paper, a detection scheme for non-cooperative signal UAVs has been proposed based on the detection of remote signals. Firstly, the closed-form solution of the optimal sampling point has been obtained, which is a function of radio environment and sensing threshold. Secondly, an adaptive detector has been provided: the sampling point of the remote signal on each subchannel adaptively varies with environmental SNR within the constrained scope. The final decision on whether the remote signal exists is made at the FC by the majority voting of multiple frequency bands. In addition, a SNR estimation scheme has been proposed, where a two-layer CNN network and a two-layer LSTM network are utilized for the accurate estimation of environmental SNR. Simulation results have validated the effectiveness of proposed method, wherein the detection accuracy was improved by about 1 dB.

Author Contributions: Conceptualization, C.W. and F.Z.; methodology, J.M.; validation, C.W., F.Z. and J.M.; formal analysis, C.W.; investigation, C.W.; data curation, C.W., W.O. and X.J.; writing—original draft preparation, C.W.; writing—review and editing, C.W., W.O., X.J. and J.M. All authors have read and agreed to the published version of the manuscript.

Funding: This research received no external funding.

Conflicts of Interest: The authors declare no conflict of interest.

References

1. Mozaffari, M.; Saad, W.; Bennis, M.; Nam, Y.; Debbah, M. A tutorial on UAVs for wireless networks: Applications, challenges, and open problems. *IEEE Commun. Surv. Tutor.* **2019**, *21*, 2334–2360. [[CrossRef](#)]
2. Zhao, N.; Cheng, F.; Yu, F.R.; Tang, J.; Chen, Y.; Gui, G.; Sari, H. Caching UAV Assisted Secure Transmission in Hyper-Dense Networks Based on Interference Alignment. *IEEE Trans. Commun.* **2018**, *66*, 2281–2294. [[CrossRef](#)]
3. Jeong, S.; Simeone, O.; Kang, J. Mobile Edge Computing via a UAV-Mounted Cloudlet: Optimization of Bit Allocation and Path Planning. *IEEE Trans. Veh. Technol.* **2018**, *67*, 2049–2063. [[CrossRef](#)]
4. Liu, D.; Xu, Y.; Wang, J.; Chen, J.; Yao, K.; Wu, Q.; Anpalagan, A. Opportunistic UAV Utilization in Wireless Networks: Motivations, Applications, and Challenges. *IEEE Commun. Mag.* **2020**, *58*, 62–68. [[CrossRef](#)]
5. Mu, J.; Jing, X.; Zhang, Y.; Gong, Y.; Zhang, R.; Zhang, F. Machine Learning-Based 5G RAN Slicing for Broadcasting Services. *IEEE Trans. Broadcast.* **2021**, *68*, 295–304. [[CrossRef](#)]
6. Mi, Y.; Jing, X.; Mu, J.; Li, X.; He, Y. DCGAN-based scheme for radar spectrogram augmentation in human activity classification. In Proceedings of the IEEE International Symposium on Antennas and Propagation & USNC/URSI National Radio Science Meeting, Boston, MA, USA, 8–13 July 2018; pp. 1973–1974.
7. Xu, X.; Zhang, X.; Yu, B.; Hu, X.S.; Rowen, C.; Hu, J.; Shi, Y. DAC-SDC Low Power Object Detection Challenge for UAV Applications. *IEEE Trans. Pattern Anal. Mach. Intell.* **2019**, *43*, 392–403. [[CrossRef](#)] [[PubMed](#)]
8. Qian, B.; Feng, Y.; Pan, C.; Tian, M. A detection method of differential frequency hopping signal based on multiple-hop autocorrelation. *Acta Aeronaut. Astronaut. Sin.* **2011**, *3*, 2268–2276.
9. Gao, X.; Li, D.; Li, N.; Chen, C. Frequency hopping signal detection algorithm based on power cancellation. *J. Nat. Sci. Univ. Jilin* **2008**, *32*, 238–243.
10. Nemsick, L.W.; Geraniotis, E. Adaptive multichannel detection of frequency-hopping signals. *IEEE Trans. Commun.* **1992**, *40*, 1502–1511. [[CrossRef](#)]
11. Wiesel, A.; Goldberg, J.; Messer-Yaron, H. SNR estimation in time-varying fading channels. *IEEE Trans. Commun.* **2006**, *54*, 841–848. [[CrossRef](#)]
12. Zhang, S.; Bao, Z. An Adaptive Spectrum Sensing Algorithm under Noise Uncertainty. In Proceedings of the IEEE International Conference on Communications, Kyoto, Japan, 5–9 June 2011; pp. 1–5.
13. Gappmair, W.; Lopez-Valcarce, R.; Mosquera, C. Cramer-Rao lower bound and EM algorithm for envelope-based SNR estimation of nonconstant modulus constellations. *IEEE Trans. Commun.* **2009**, *57*, 1622–1627. [[CrossRef](#)]
14. Abeida, H. Data-Aided SNR Estimation in Time-Variant Rayleigh Fading Channels. *IEEE Trans. Signal Process.* **2010**, *58*, 5496–5507. [[CrossRef](#)]
15. Mu, J.; Tan, Y.; Xie, D.; Zhang, F.; Jing, X. CNN and DCGAN for Spectrum Sensors over Rayleigh Fading Channel. *Wirel. Commun. Mob. Comput.* **2021**, *2021*, 9970600. [[CrossRef](#)]
16. Yang, K.; Huang, Z.; Wang, X.; Wang, F. An SNR Estimation Technique Based on Deep Learning. *Electronics* **2019**, *8*, 1139. [[CrossRef](#)]
17. Sun, Y.; Zeng, G.; Liu, C.; Zhang, D. SNR estimation algorithm for UAV data link based on deep learning. *J. Beijing Univ. Aeronaut. Astronaut.* **2019**, *45*, 1855–1863.
18. Mu, J.; Zhang, F.; Cui, Y.; Zhu, J.; Jing, X. Non-cooperative UAV detection with adaptive sampling of remote signal. In Proceedings of the 2021 International Wireless Communications and Mobile Computing (IWCMC), Harbin, China, 28 June–2 July 2021; IEEE: New York, NY, USA; pp. 791–795.
19. Liang, Y.; Zeng, Y.; Peh, E.C.Y.; Hoang, A.T. Sensing-Throughput Tradeoff for Cognitive Radio Networks. *IEEE Trans. Wirel. Commun.* **2008**, *7*, 1326–1337. [[CrossRef](#)]
20. Hengy, S.; Laurenzis, M.; Hommes, A.; Christnacher, F. Multimodal UAV detection: Study of various intrusion scenarios. In Proceedings of the Electro-optical Remote Sensing, Warsaw, Poland, 11–12 September 2017; SPIE: Bellingham, WA, USA, 2017; Volume 10434, p. 104340.
21. Shi, S.; Schubert, M.; Boche, H. Downlink MMSE Transceiver Optimization for Multiuser MIMO Systems: Duality and Sum-MSE Minimization. *IEEE Trans. Signal Process.* **2008**, *56*, 3702–3712. [[CrossRef](#)]
22. Gronemeyer, S.A.; Mcbride, A.L. MSK and Offset QPSK Modulation. *IEEE Trans. Commun.* **2003**, *24*, 809–820. [[CrossRef](#)]
23. Szeto, V.F.; Pasupathy, S. Iterative decoding of serially concatenated convolutional codes and MSK. *IEEE Commun. Lett.* **2002**, *3*, 272–274. [[CrossRef](#)]
24. Chin, K.; Siu, A.; Ying, S.; Zhang, Y. Da Jiang Innovation, DJI: The Future of Possible. *Acad. Asian Bus. Rev.* **2017**, *3*, 83–109. [[CrossRef](#)]